1-10-2004

High-Resolution Chandra Spectroscopy Of Gamma Cassiopeiae (B0.5e)

M. A. Smith

David H. Cohen
Swarthmore College, dcohen1@swarthmore.edu

M. F. Gu

See next page for additional authors

Recommended Citation

Authors

M. A. Smith, David H. Cohen, M. F. Gu, R. D. Robinson, N. R. Evans, and Prudence G. Schran

HIGH-RESOLUTION *CHANDRA* SPECTROSCOPY OF γ CASSIOPEIAE (B0.5e)

MYRON A. SMITH

Catholic University of America and Computer Sciences Corporation/STScI, 3700 San Martin Drive, Baltimore, MD 21218; msmith@stsci.edu

DAVID H. COHEN

Department of Physics and Astronomy, Swarthmore College, 500 College Avenue, Swarthmore, PA 19081

MING FENG GU[1]

Center for Space Research, Massachusetts Institute of Technology, 70 Vassar Street, Cambridge, MA, 02139

RICHARD D. ROBINSON

Catholic University of America and Computer Sciences Corporation/Johns Hopkins University, 3400 North Charles Street, Baltimore, MD 21218

NANCY REMAGE EVANS

Center for Astrophysics, Harvard University, 60 Garden Street, Cambridge, MA 02138

AND

PRUDENCE G. SCHRAN

Department of Physics and Astronomy, Swarthmore College, 500 College Avenue, Swarthmore, PA 19081

ABSTRACT

γ Cas is the prototypical classical B0.5e star and is now known to be the primary in a wide binary system. It has long been famous for its unique hard X-ray characteristics, among which are variations that correlate with changes in a number of optical light and UV line and continuum properties. These peculiarities have led to a picture in which processes on or near the Be star produce the observed X-ray emission. In this paper we report on a 53 ks *Chandra* High Energy Transmission Grating Spectrometer observation of this target. An inspection of our spectrum shows that it is quite atypical for a massive star. The emission lines appear weak because of a strong short-wavelength continuum that arises from a hot plasma with $kT = 11$–12 keV. The spectrum exhibits many lines, the strongest of which are Lyα features of H-like species from Fe through the even-Z intermediate elements (S, Si, Mg, and Ne), down to O and N. Line ratios of the "*rif* triplet" for a variety of He-like ions and of Fe XVII are consistent with the dominance of collisional atomic processes. However, the presence of Fe and Si fluorescence K features indicates that photoionization also occurs in nearby cold gas. The line profiles indicate a mean velocity at rest with an rms line broadening of 500 km s^{-1} and little or no asymmetry. An empirical global-fitting analysis of the line and continuum spectrum suggests that there are actually three or four plasma emission components. The first is the dominant hot (12 keV) component, of which some fraction (10%–30%) is heavily absorbed, while the remainder is affected by a much lower column density of only 3×10^{21} cm^{-2}. The hot component has a Fe abundance of only 0.22 ± 0.05 solar. The other two or three major emission components are "warm" and are responsible for most other emission lines. These components are dominated by plasma having temperatures near 0.1, 0.4, and 3 keV. Altogether, the warm components have an emission measure of about 14% of the hot component, a low column density, and a more nearly solar composition. The 100 eV component is consistent with X-ray temperatures associated with a wind in a typical early B star. Nonetheless, its emission measure is a few times higher than would be expected from this explanation. The strength of the fluorescence features and the dual-column absorption model for the hot plasma component suggest the presence near the hot sites of a cold gas structure with a column density of $\sim 10^{23}$ cm^{-2}. Because this is also the value determined by Millar and Marlborough for the vertical column of the Be disk of γ Cas, these attributes suggest that the X-ray–emitting sources could be close to the disk and hence to the Be star. Finally, we discuss the probably related issues of the origin of the warm emission components, as well as the puzzling deficient Fe abundance in the hot component. It is possible that the latter anomaly is related to the FIP (abundance fractionation) effect found in certain coronal structures on the Sun and RS CVn stars. This would be yet another indication that the X-rays are produced in the immediate vicinity of the Be star.

Subject headings: circumstellar matter — stars: emission-line, Be — stars: flare — stars: individual (γ Cassiopeiae) — X-rays: stars

1. INTRODUCTION

γ Cas (B0.5 IV) has held a unique place among the broad group of X-ray–emitting OB stars because of its extensive and unusually dense ($n_e \simeq 10^{13}$ cm^{-3}; Waters, Cote, & Lamers 1987) decretion disk and the attributes of its X-ray emission. The disk has been imaged in Hα out to several stellar radii, and its ellipsoidal shape permits an estimate of the orientation angle of the disk and rotation plane with respect to the line of sight, $\simeq 46°$ (Quirrenbach et al. 1997). Its various X-ray properties are peculiar and virtually unique for a massive star. First, its X-ray luminosity [$(0.4$–$1.1) \times 10^{33}$ ergs s^{-1}] is midway between the

L_X values of normal B and classical Be stars on the low side and X-ray Be binaries on the high side. The X-rays are also thermal, but with an extremely high temperature of $kT = 10.5–12$ keV. Several investigators have attempted to explain this property by wind or Be disk infall onto a degenerate companion, generally a white dwarf (see Kubo et al. 1998; Owens et al. 1999; Apparao 2002). Potentially, this picture can explain in a general way the hard thermal spectrum of the X-rays. However, while the star is now established as part of a binary system (see Harmanec et al. 2000; Miroshnichenko, Bjorkman, & Krugov 2002), the wide separation ($P ≈ 204$ days, with low to moderate eccentricity) makes it difficult to understand the high L_X if the companion were a white dwarf. Moreover, for a companion to have evolved to a degenerate star, it must have initially been more massive than γ Cas and would more likely have developed into a neutron star than a white dwarf. A neutron star system can easily explain the L_X but not the presence of dominant thermal processes implied by the continuum shape and the presence of Fe xxv and xxvi lines. The spectra of Be–neutron star (Be-NS) binary systems generally tend to be nonthermal and show a strong fluorescence feature near 6.5 keV, which is not seen in γ Cas (Kubo et al. 1998). In addition, neutron star systems generally have a strong tendency to have eccentric orbits and to show periodic X-ray pulses, unlike γ Cas.

Smith, Robinson, & Corbet (1998a, hereafter SRC98) have shown that there are actually two components to the hard X-rays, each having about the same temperature. One is characterized by rapid fluctuations (flares or "shots") lasting from a few seconds (or less) to a few minutes. These must be emitted from a high-density optically thin plasma. The second, "basal" component (also optically thin), varies on a timescale of hours and contributes 60%–70% of the total flux. SRC98 found that the basal X-ray variations were anticorrelated with UV continuum variations near 1400 Å and proposed that the X-rays were actually coming from near γ Cas itself. In their model they proposed that the shots were emitted by violent flares at the top of the photosphere of the Be star. These exploding parcels expand with rather little energy loss and fill a lower density cavity inside supposed magnetic loops emerging from the star's surface, which is the site of the basal emission. These filled cavities are thought to be associated with corotating clouds of cool material, which are responsible for striated subfeatures in time series spectra of optical and UV line profiles, as well as variations in the thermal properties of UV spectral lines (Smith & Robinson 1999; Cranmer, Smith, & Robinson 2000, hereafter CSR00) and absorptions in the UV continuum light curves (Smith, Robinson, & Hatzes 1998b, hereafter SRH98). Highly redshifted spectral lines in the UV (Smith & Robinson 1999) are indicative of high-velocity plasmoids, with energies comparable to the X-ray flux and suggest the interaction of X-ray–emitting volumes with a circumstellar structure, probably the dense disk of the Be star. There is indirect evidence from both UV–X-ray correlations (CSR00) and broad high-level hydrogen lines (Waters et al. 2000) that this interaction occurs in a region where circumstellar gas ceases to corotate at the angular rate of the star's surface and begins to follow a Keplerian orbital relation.

Recently, evidence for the star's disk being somehow associated with the X-ray generation entered the picture with the discovery by Robinson, Smith, & Henry (2002, hereafter RSH02) of correlated optical–X-ray cycles with a mean length of 70 days. The amplitudes of the variations are a factor of 3 for the X-ray and 3% for optical flux. Yet because of the small contribution of the X-ray emission to the star's total luminosity, the optical variations cannot be produced by reprocessing X-ray flux, and thus the optical variations must have another cause. The association of these variations with the disk is implied by their slightly reddish color, which probably means that they come from a source cooler than the Be star. Finally, the *cyclical* nature of the variations led RSH02 to suggest a dynamo origin. Thus, this work has potentially placed the generation of the X-rays into a comprehensive (although otherwise untested) picture in which the X-ray and optical variations result from magnetic stresses between the star and the disk.

The X-ray properties of this star and continued questions about the nature of its emission have made it a natural target for spectroscopy. A high-resolution spectrum permits a description of the temperatures, densities, and kinematics of the X-ray–emitting regions. At a more qualitative level, an X-ray spectrum makes possible a comparison with the spectra of other well-known systems, such as accreting white dwarfs and neutron stars, and the determination of whether its spectral characteristics are as peculiar as its temporal and flux properties. To address these issues, we requested and were granted time with the High and Medium Energy Transmission Gratings (HEG and MEG) of the *Chandra* satellite. We report herein on our analysis of this spectrum.

2. OBSERVATIONS AND REDUCTION

Our HEG/MEG spectra were obtained with a 52.5 ks exposure time starting 2001 August 10, 0921 UT. We have reextracted the MEG and HEG spectra and created the ancillary response file and response matrix file by using *CIAO* version 2.3 and *CALB* version 2.18. This brought any shifts between the plus and minus spectral orders below levels of detection ($±0.2$ pixel), which was not the case in the original pipeline extraction.

The analysis of the line strengths and significances and the determination of plasma emission properties were carried out with Interactive Spectral Interpretation System (ISIS) tasks. The parameters were determined for each of the four spectra, leading to a weighted average of the measurements. The determination of radial velocities and line widths was carried out independently using a variety of *ISIS, Sherpa,* and *IDL* routines, with all approaches leading to consistent results.

3. ANALYSIS

3.1. *Photometric Time History*

Our observation was conducted at an epoch when γ Cas had just gone through a minimum in its ∼70 day flux cycle and had an X-ray flux close to its average value. A light curve during the observation was extracted from HEG and MEG $m = −1$ and $+1$ fluxes. We chose a bin size of 60 s as a compromise between the effects of photon quantization and the loss of individual shot events. The resulting light curve is shown in Figure 1. The plot shows a typical meandering pattern of the fluxes with variations on a timescale of a few hours. This pattern is typical of a few weakly undulating light curves previously seen, such as the 1998 and 2000 *RXTE "Visit 1"* given by RSH02. It is quite different from those in which a slow, probably rotationally induced, modulation dominates and clear maxima and minima can be identified. Possible dips at $≤0$, 6, and 14 hr are reminiscent of the 7.5 hr cycle discovered by Robinson & Smith (2000). The cause of this cyclicity (which may not always recur with a cycle length of 7.5 hr) is unknown. Nonetheless, this phenomenon appears
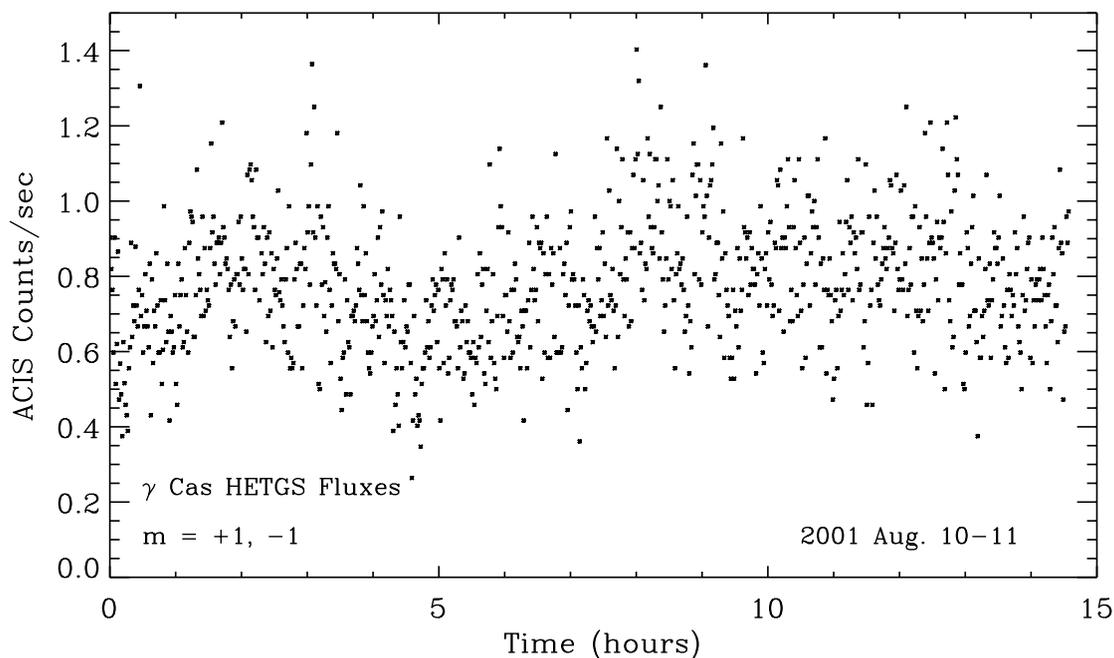
Fig. 1.—Light curve of γ Cas extracted from our first-order HETGS spectra and binned to 1 minute averages

robust in most *RXTE* data (RSH02). It was also visible as periodic absorptions in the blue wings of C IV and Si IV resonance lines in archival *IUE* spectra (CSR00).

To see whether these flux variations might translate to changes in spectral line strengths, we divided the time sequence into regions of high and low flux and generated X-ray spectra from each group. The resulting spectra were rather noisy and showed no statistically significant changes. This is consistent with results presented by SRC98 and Smith & Robinson (1999), who showed that *RXTE* spectra of the shots was generally similar to that of the basal component.

Figure 1 also shows that the lower and upper envelopes correspond quite well, with the upper envelope being only occasionally interrupted by shots lasting 3–4 minutes (e.g., at 3.1 and 8 hr). Tests with truncated and noise-added renditions of some of our past *RXTE* light curves show that these properties are not unusual. Thus, we believe that the envelope correlations and absence of all but a few long-lived shots are probably simply artifacts of the low count rate.

3.2. *General Reconnaissance of Spectrum*

Figure 2 exhibits the complete MEG/HEG spectrum of γ Cas in flux units over the range 1.6–25 Å, weighted by the wavelength and detector dependences in effective aperture and binned every 10 mÅ. The continuum is strong at the high-energy end, which in thermal plasmas indicates a hot-plasma free-free emission component, and it also exhibits significant attenuation at wavelengths above 12 Å. The spectrum is also sprinkled with a number of emission lines, the properties of which are listed in Table 1. The presence of these lines indicates a broad distribution of ion stages, ranging from Fe^{25+} on the high side down to N^{6+}. The most prominent lines are those of Fe XXV and Fe XXVI, which have been observed by Kubo et al. (1998). These lines are weak relative to the underlying continuum or with respect to lines in other ~10 keV sources. Most of the other lines present are Lyα lines of H-like even–atomic number elements, ranging from sulfur to oxygen (but

also including N VII), with one or two Lyβ lines also being present. Various density indicators are present weakly, including lines of (He-like) Si XIII, Ne IX, and O VII, as well as a possible weak blend of the Fe XVII density diagnostic at 17.05 and 17.10 Å. A weak fluorescent K feature of Si at 7.1 Å, as well as a moderate-strength emission at 1.9 Å, arising from the analog Fe K feature, is also present. These are the sole visible diagnostics of plasma photoionization processes compatible with a hot plasma in the data.

We ran our spectrum through customized programs, as well as ISIS software, to determine the significance of spectral features. The identification of weak lines of a common ion was guaranteed by their simultaneous evaluation at predicted wavelengths or in the case of individual weak features (e.g., Ne X, Lyβ, and N VII Lyα) from strengths of lines of various ions along H-like or He-like electronic sequences, including Ne IX and O VII.

3.3. *Line Kinematics*

To assess the kinematic properties of the line-emitting plasma, we chose several strong and unblended lines of H-like Fe, S, Si, Mg, Ne, and O for detailed study. In measuring the radial velocity and nonthermal broadening of the strongest spectral lines of γ Cas, we found agreement from two techniques, first, by using appropriate Gaussian-fitting routines and, second, by performing a cross-correlation and convolution of the profiles of these lines in an archival spectrum of AB Dor with respect to our γ Cas data. The resulting centroid wavelengths, standard deviation, Gaussian-fitted line center, and continuum fluxes are listed in Table 1. The measured wavelengths indicate no systematic radial velocity for the emission region.

The line widths are all consistent with a Gaussian velocity distribution of $\sigma_v = 478 \pm 50$ km s^{-1}. The error bars for the Fe XXV and XXVI lines are considerably larger, and we estimate these to be ± 325 km s^{-1}. No statistically robust evidence was found for asymmetries in the line profiles. However, because
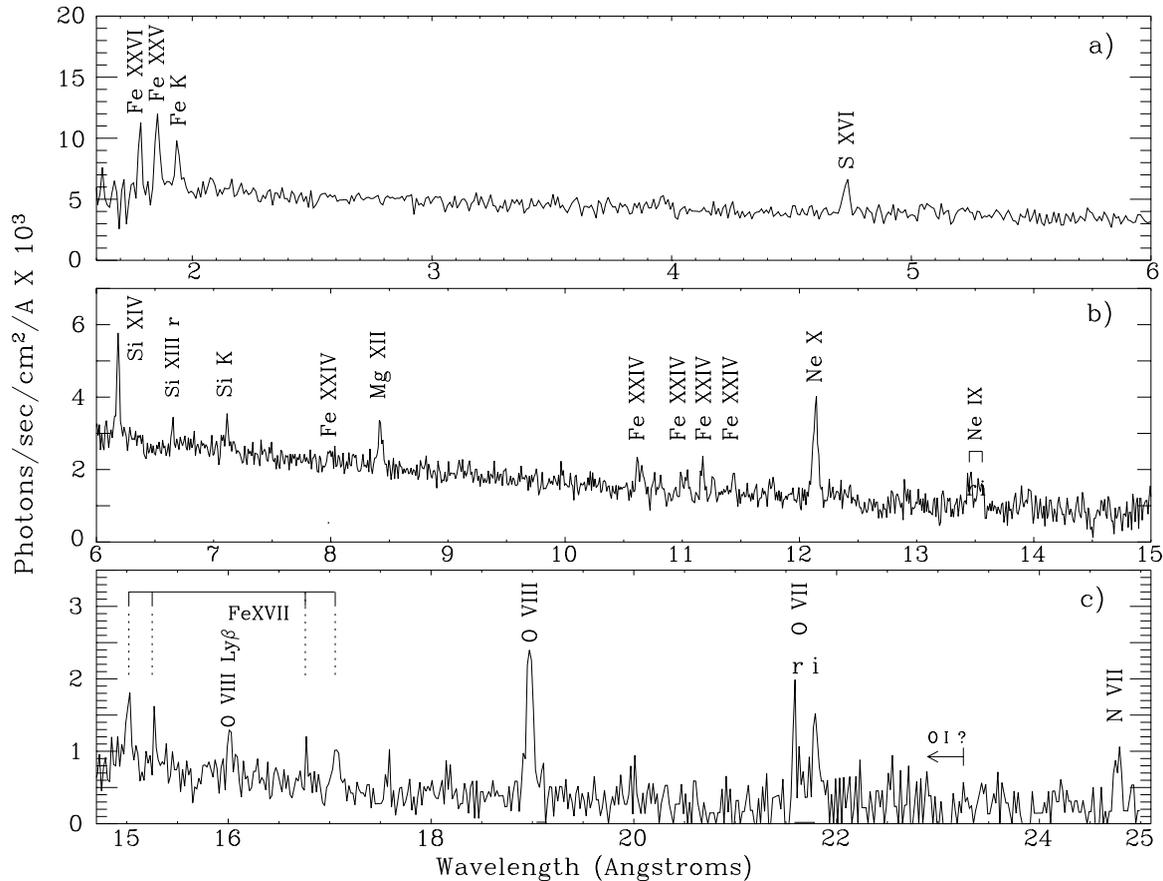
Fig. 2.—Combined HEG-MEG spectrum of γ Cas from all four first-order detectors, binned to 10 mÅ. Lines studied in this paper are indicated.

there is a hint of stronger wings than indicated by Gaussian fits among the stronger Lyα lines, we cannot rule out the possibility of a second kinematic component with a larger broadening velocity.

To determine the fluxes of weaker lines, such as those of iron L-shell ions, we perform similar Gaussian fits by fixing their wavelengths at the known theoretical values and the velocity broadening obtained from the fit to strong lines mentioned above. The line fluxes and continuum level at the line centers are also listed in Table 1. The equivalent widths in angstrom units can be computed by dividing the line fluxes by the continuum fluxes.

3.4. *Global Spectral Analysis*

3.4.1. *Basic Model M1*

To derive the thermal properties of the plasma, we chose to use global-fitting techniques to constrain the emission measure distribution of the plasma. We utilized the Astrophysical Plasma Emission Code (APEC), as implemented in ISIS, to perform the spectral fitting. From previous X-ray satellite observations of γ Cas, we know that the continuum emission can be described by a heavily absorbed bremsstrahlung with temperature $\simeq 10$ keV. The high spectral resolution of the High Energy Transmission Grating Spectrometer (HETGS) clearly demonstrates the existence of more complex emission measure structure at lower temperatures, although the overall continuum seems to be dominated by the $\simeq 10$ keV component. Within the HETGS bandpass we found that the temperature and the absorption column density are somewhat

degenerate. Therefore, we constrained our spectral analysis to contain a hot component with a fixed temperature of 12.3 keV, as determined by the broadband *BeppoSAX* observations (Owens et al. 1999). We consider the errors on this parameter to be about ± 1 keV. As Table 2 shows, the value of 12.3 keV is generally consistent with the previously reported temperature determinations.

The presence of relatively strong Fe XXIII and XXIV lines and the ratio of the Fe XVII 15 to 17 Å lines (see, e.g., Kinkhabwala et al. 2002), as well as the values of the He-like triplet G-ratios $[(i+f)/r]$ of Ne IX and O VII, are all consistent with collisionally ionized plasma. These ratios are also consistent with a photoionized plasma if the photoexcitations contribute significantly to the resonance lines (Kinkhabwala et al. 2002). However, the latter condition does not seem to apply to the observed spectrum, since this would also require much larger high-*n* series line fluxes for H-like and He-like ions populated by photoexcitation, in contradiction to the almost nonexistent Heβ line of O VII (18.6 Å) and the only weak Lyβ line of O VIII (16.0 Å) in the data. The absence of detectable radiative recombination continuum features (e.g., for S XVI at 3.5 Å, for Si XIV at 4.6 Å, for Mg XII at 6.4 Å, for Ne X at 9.3 Å and for O VIII at 14.2 Å) is also inconsistent with photoionization models. Therefore, we pursue only the collisional models to explain the hot plasma below.

From the presence of lines from both Fe L-shell and O VII–VIII ions, it is clear that emission regions also exist with temperatures from a few keV down to ~ 100 eV. As a first attempt to characterize the differential emission measure (DEM) in this regime, we chose a four-component thermal and optically thin

TABLE 1
MEASURED LINE PROPERTIES

Ion	λ_{th} (Å)	λ_{obs} (Å)	σ_λ (mÅ)	Line Flux (10^{-5} photons cm^{-2} s^{-1})	Continuum Flux (10^{-3} photons cm^{-2} s^{-1} Å^{-1})
Fe XXVI Lyα	1.780	1.7816 (14)	2.3 ± 2.0	10.6 ± 2.1	5.44
S XVI Lyα	4.729	4.7295 (12)	9.4 ± 1.7	8.6 ± 1.2	3.96
Si XIV Lyα	6.182	6.1848 (11)	8.4 ± 1.1	7.8 ± 0.5	2.96
Mg XII Lyα	8.421	8.4216 (23)	14.8 ± 3.2	4.9 ± 0.7	2.10
Ne X Lyα	12.134	12.1374 (15)	18.8 ± 1.9	12.6 ± 1.6	1.26
O VIII Lyα	18.969	18.9756 (67)	32.0 ± 6.0	17.1 ± 2.6	0.49
Fe XXV r	1.8504	...	2.9	6.8 ± 1.9	6.1
Fe XXV i	1.8570	...	3.0	5.7 ± 1.8	6.0
Fe XXV f	1.8682	...	3.0	2.4 ± 1.5	5.9
Fe I Kα_1	1.9358	...	3.1	3.6 ± 1.8	6.2
Fe I Kα_2	1.9398	...	3.1	5.0 ± 1.5	6.2
Si XIII r	6.6479	...	10.6	2.0 ± 0.5	2.6
Si XIII i..................	6.6850	...	10.6	0.6 ± 0.5	2.6
Si XIII f..................	6.7395	...	10.7	0.9 ± 0.4	2.6
Mg XI r..................	9.1687	...	14.6	0.9 ± 0.7	1.8
Mg XI i	9.2300	...	14.7	0.2 ± 0.4	1.8
Mg XI f..................	9.3136	...	14.8	0.0	1.8
Ne IX r..................	13.447	...	21.4	4.3 ± 0.9	0.96
Ne IX i	13.551	...	21.6	4.5 ± 1.3	0.96
Ne IX f..................	13.698	...	21.8	0.0	0.95
Fe XXIV..................	10.622	...	16.9	3.1 ± 0.6	1.4
Fe XXIV..................	10.663	...	17.0	1.9 ± 0.6	1.4
Fe XXIV/XXIII.............	11.029	...	17.6	2.7 ± 0.6	1.3
Fe XXIV..................	11.266	...	17.9	1.6 ± 0.8	1.3
Fe XVII	15.014	...	23.9	5.9 ± 1.7	0.93
Fe XVII	15.266	...	24.3	1.5 ± 1.3	0.92
O VIII Lyβ...............	16.006	...	25.5	3.1 ± 1.6	0.74
Fe XVII	16.780	...	26.7	2.4 ± 1.2	0.54
Fe XVII	17.051	...	27.2	3.3 ± 1.8	0.48
Fe XVII	17.096	...	27.2	1.8 ± 1.3	0.47
O VII r....................	21.602	...	34.4	7.7 ± 2.8	0.34
O VII i....................	21.802	...	34.7	7.9 ± 4.0	0.33
O VII f....................	22.097	...	35.2	1.3 ± 1.6	0.31
N VII Lyα	24.789	...	39.5	6.1 ± 2.6	0.26

model, which we call M1, to explain the main characteristics of the line and continuum emission. Each temperature is restricted to a certain range to represent the characteristic emission lines. Although the temperature of the dominant hot component was fixed at $kT_1 = 12.3$ keV, the value of the second component was permitted to float within the range 1–4 keV. This condition was imposed by the presence of Fe XXIII and XXIV lines at 10–11 Å. The third component has a temperature between 300 and 1 keV, as suggested by the relatively strong Fe XVII, Ne IX, and Ne X lines. The fourth component has a temperature near 100 eV and accounts for the O VII and N VII lines. We refer to components 2–4 as "warm" plasmas in our discussion below. To summarize, the requirements for four components are determined by lines arising from ions having ionization potentials in different ranges, which in turn correlate very well with wavelength. Thus, we may say that component 1 is determined by the hard continuum and the ratio of the two Fe K lines (<1.8 Å) and components 2, 3, and 4 by lines in the ranges 1.8–11.9, 12–20, and >20 Å, respectively. This is illustrated for our model 2 in Figure 3b', which is discussed below.

Previous satellite missions have found that the measured Fe XXV and XXVI line intensities require a significantly subsolar

TABLE 2
X-RAY–DERIVED VALUES OF kT AND COLUMN DENSITY

Author	Satellite	kT (keV)	Fe/Fe$_\odot$	N_{H} (cm^{-2})
Murakami et al. 1986	*Tenma*	11.7 ± 0.8	0.3 ± 0.1	1.3×10^{22}
Parmar et al. 1993	*EXOSAT*	8.2 ± 0.09	0.26 ± 0.5	1.5×10^{21}
Kubo et. al. 1998....................	*ASCA*	10.7 ± 0.6	0.35 ± 0.08	$(1.5 \times 10^{21}) \pm 0.1$
SRC98..	*RXTE*	$10.5 \pm 0.4, 11.8 \pm 0.4$	0.35 ± 0.1	...
Robinson & Smith 2000..........	*RXTE*	$(10.8–11.4) \pm 0.2$	0.34 ± 0.1	2×10^{22}
Owens et al. 1999....................	*BeppoSAX*	12.3 ± 0.6	0.42 ± 0.05	$(1.55 \times 10^{21}) \pm 0.09$
This paper	*Chandra*	...	$0.22 – 0.26$	5×10^{21}

Fe abundance (see Table 2). Therefore, we decoupled the Fe abundance in the hot component from the abundances of all metals (including Fe) in the warm components. The measured line strengths probably have errors of $\pm 10\%$–15% and largely determine the uncertainty of the Fe abundance for the hot component, which we take as $\pm 20\%$. The uncertainty in the abundance estimates of the other elements is sensitive to the details of DEM models and may be even larger. In model M1 all four components are affected by a common absorption column density and have the same velocity broadening with the width fixed at the value derived in the previous section. In our models each component has three unknowns (temperature, abundance, and column density). Since in model M1 we tie together the column densities and separate Fe from other metallic abundances in the hot component, we end up formally with 10 free parameters. A joint fit to the ± 1 orders of HEG and MEG spectra was carried out with ISIS, making use of Cash statistics to take into account the small number of counts in the long-wavelength region.
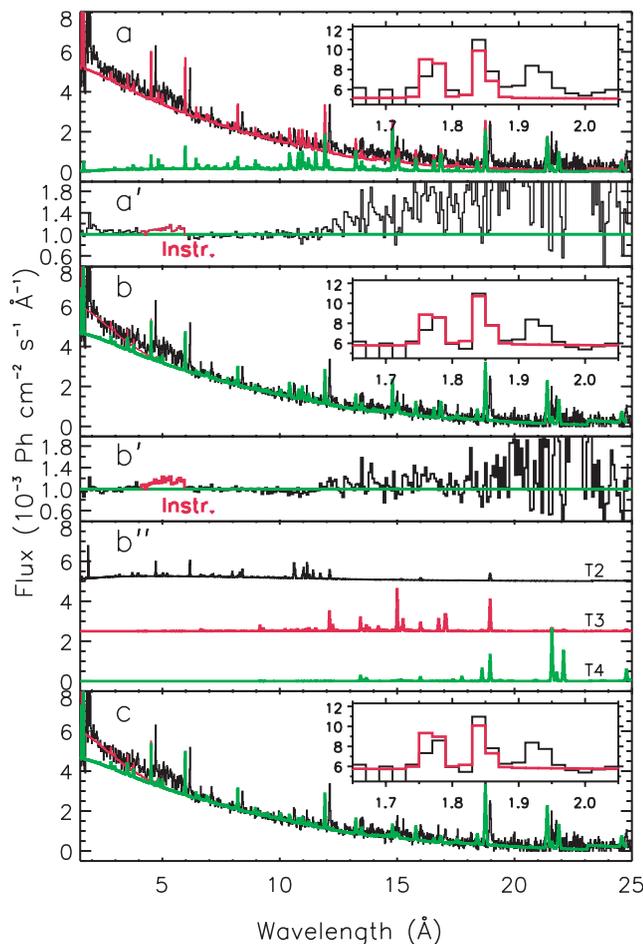
The best-fit parameters for model M1 are shown in Table 3. Because we are concerned only with the overall temperature structure of the plasma and we do not expect the simple models discussed here to be statistically acceptable across the entire HEGS bandpass, we have not attempted to derive statistical uncertainties of all the best-fit model parameters. Formal errors that one could calculate from line and continuum discrepancies, which are themselves highly interdependent, do not reflect the probably larger errors inherent in the qualitative representation of the geometry envisaged for the X-ray sites near γ Cas. The input geometries can be quite diverse, depending, for example, on the proximity to and association of the X-ray emission centers with the Be disk and also their distribution over the Be star's surface. In addition to geometric considerations, the emission mechanisms associated with a supposed degenerate companion could be even more different and thus more elusive to quantify. To give the reader a flavor of the likely range of parameters within the context of the Be star-disk model of X-ray emission, we report results for three models. We represent the errors for most parameters in terms of the measured difference between the M1 and the M2 model discussed below. We also exhibit the comparison between each model and data in Figure 3a graphically. For illustration purposes, the ± 1 orders of HEG and MEG spectra are rebinned to 0.02 Å bin size and co-added.

As expected, the emission measure and spectrum below $\simeq 6$ Å are dominated by the hot component. Note from the insets in Figure 3 that the Fe line ratio for the hot component fits the observations reasonably well, strengthening the conclusion that the dominant plasma emission processes are thermal. Note also the clear presence of the Fe K fluorescence feature, which is not included in the APEC model. In our first model, M1, we find an Fe abundance of only 0.34 for the hot component, in agreement with the findings of previous X-ray missions (Table 2). The abundances of the metallic elements in the warm components are constrained by the strengths of the Lyα lines of H-like and He-like ions. The overall good agreement between the solar abundance model and data for these lines indicates that the metallic abundances of the warm component are significantly closer to solar values than Fe is in the hot component.

One obvious mismatch in model M1 is the He-like triplet line ratios of O and Ne, and our discussion of these is deferred to § 3.6. Besides the continuum discrepancy in the 4–6 Å region, which may well be attributed to the known calibration problem in the effective area of *Chandra* mirror assembly, two additional spectral regions can be easily identified from Figure 3a where the model continuum level is significantly lower than the data. The first is the region between 2 and 2.5 Å, and the second is at $\gtrsim 12$ Å. The green line in Figure 3a shows the contribution from the three warm components. It is clear that the continuum flux from this component is too small to account for the deficit. The shallower slope of the observed continuum near 12 Å indicates that the absorption column density may be lower than what is derived from model M1. Yet, a lower column density would worsen the discrepancy in the 2–3 Å region where the observed continuum slope is steeper than the model.

3.4.2. *Two-Column Density Models (Hot Component)*

One can avoid this problem by varying the column density absorptions of the dominant emitting components. This can be done in one of two ways. In the first case, one can increase the column density for the hot component and decrease the column

Fɪɢ. 3.—Comparison of best-fit models and the data: (*a*) model M1; (*b*) model M2; (*c*) model M3. In all panels, the line depicts the data. Red is the best-fit model, shifted by -0.2 Å for clarity. In (*a*), green is the contribution from the components T_2, T_3, and T_4, also shifted by -0.2 Å. In (*b*) and (*c*), red is the sum of all components, while green is the sum of all components (T_1–T_4) having the "low" column density $\approx 3 \times 10^{21}$ cm^{-2}. (*a′*–*b′*) Data-to-model ratio for models M1 and M2. (*b′*) Individual spectra (unshifted) for components T_2, T_3, and T_4 of Model 2. The insets show the Fe xxvɪ and xxv line region in detail; the obvious mismatch of the fluorescence feature at 1.9 Å is discussed in the text. Note that the 4–6 Å region is not well calibrated because of an iridium spectral edge from the telescope mirror coating.

TABLE 3
Fɪᴛ Pᴀʀᴀᴍᴇᴛᴇʀs

Parameters	M_1	M_2	M_3	Error
kT_1 (keV)........................	12.3	12.3	12.3	...
$NORM_1$[a]........................	0.112	0.134	0.135	± 0.022
EM_1 (10^{54} cm³)[b]	47	57	57	± 10
kT_2 (keV)........................	1.86	3.08	2.50	± 1.2
$NORM_2$	0.0071	0.011	0.012	± 0.004
EM_2 (10^{54} cm³).............	3.0	4.6	5.1	± 1.6
kT_3 (keV)........................	0.370	0.375	0.393	± 0.005
$NORM_3$	0.0032	0.0023	0.0026	± 0.0009
EM_3 (10^{54} cm³).............	1.4	1.0	1.1	± 0.4
kT_4 (keV)........................	0.135	0.146	0.148	± 0.011
$NORM_4$	0.014	.0088	0.0092	± 0.005
EM_4 (10^{54} cm³).............	5.9	3.7	3.9	± 2.2
ABUND(Fe)[c]	0.34	0.22	0.26	± 0.05
ABUND	1.1	0.81	0.77	± 0.3
N_H (10^{21} cm⁻²)[d]...........	3.7	2.7	2.7	± 1.0

[a] For M2 and M3, NORM1 is the total normalization of the two hot subcomponents, each having a different absorption.
[b] A *Hipparcos* distance of 188 pc is assumed (ESA 1997).
[c] For M1 and M2, ABUND(Fe) is the iron abundance of the hot components alone. For M3, this is the iron abundance of both hot and warm components, which are tied together.
[d] For M1 this is the column density for all components, for M2 and M3, the column density for the kT_2, kT_3, and kT_4 component and 75% of the hot subcomponent kT_1.

densities of the warm ones to compensate for the flux attenuation where needed. This procedure required only a slight increase in the column density of the hot component but resulted in a decrease of the warm-component column to effectively zero. However, these changes slightly reduced the continuum flux below 10 Å and raised the fluxes at long wavelengths. Even so, the corrections were not sufficient and still generated an undercorrection in the 12–16 Å region. We were able to produce a better fit by splitting the hot component into two subcomponents, one with a rather high column density of 10^{23} atoms cm⁻² (a value to be justified later), and a second one, with a lower, floating column density, which is tied to the attenuation of the warm components. Note that a column density of 10^{23} atoms cm⁻² transmits nearly all short-wavelength (≤4 Å) flux while at the same time effectively absorbing flux above 12 Å. We allowed the volume ratio of the more absorbed to less absorbed hot subcomponents to vary freely, and this value floated to 15%. However, we found that fractions as high as 30% or as low as 10% also give acceptable fits. On the basis of these results, we modified the model M1 to produce a model M2 with a fraction of 25% for the high column density subcomponent and 75% for the low column density subcomponent (this causes minor adjustments in some of the other fit parameters). This is exhibited as a sketch in Figure 4. The best-fit parameters are listed in Table 3, and the comparison between the model and data are shown in Figure 3*b*. This model gives a significantly better fit to the data than M1. The extra, more heavily absorbed hot component not only fills in the continuum deficit near 2 Å, but it also allows the other plasma components to take on a slightly lower column density, 2.7×10^{21} cm⁻², thereby removing the disagreement in the longer wavelength regions. The various predicted line emissions appear to agree with the data satisfactorily as well. We note that in M2 the Fe abundance is decreased to 0.22, mainly from the Fe xxv and xxvi lines. We note that the model fluxes are slightly high for the Fe xvii lines. However, such small discrepancies can be easily attributed to our oversimplified DEM models.

In the models M1 and M2, we have tied the iron abundance in the warm components to the other metallic elements. It is interesting to investigate whether it is possible that the iron abundance in both hot and warm components are the same and very subsolar. For this purpose, we constructed a model M3, which is identical to M2 except that the iron abundance of the warm component is tied to the value determined for the hot one (now 0.26) and is independent of other metallic abundances. Of these three models, M2 gives the best overall fit, and thus we adopt it. The best-fit parameters for all three models are listed in Table 3 and the comparisons between the models and data are shown in Figure 3*c*. It is evident that for M3 the Fe L-shell lines, especially the Fe xxiii and xxiv lines, are underpredicted from the low trial iron abundance. This low Fe value is required by the Fe xxv and xxvi lines in our data and by observations of other satellites (see Table 2). Therefore, we conclude that the iron abundance in the warm component is close or equal to the solar value.

The difference in Fe abundance of the hot and warm components argues strongly that these plasmas are not cospatial. Additionally, the hot component must be fairly sharply peaked at ≥10 keV, or it would overpredict the Fe xxiii and xxiv line strengths, even with the low Fe abundance. It is not clear whether the first two warm components are distinct from each other or whether the third warm component is distinct from these other two. We have also experimented with a power-law DEM component for the temperature range 0.5–3 keV, which fits the data as well as M2. The quality of data does not enable us to differentiate a smooth temperature distribution or several discrete temperatures for the warm components. However, a single power-law DEM model that includes the hot component fails to describe both continuum and line emission satisfactorily. Thus, for simplicity's sake, we have adopted the multitemperature thermal models as the preferred analysis method.

It is worth mentioning that a strong neutral oxygen absorption edge at 23.05 Å is predicted in all our models. Because the continuum level at this wavelength is very low and the HEGS effective area is small, the statistical quality of the data does not allow for a straightforward analysis of this feature. Nevertheless, we may still carry out a statistical test to
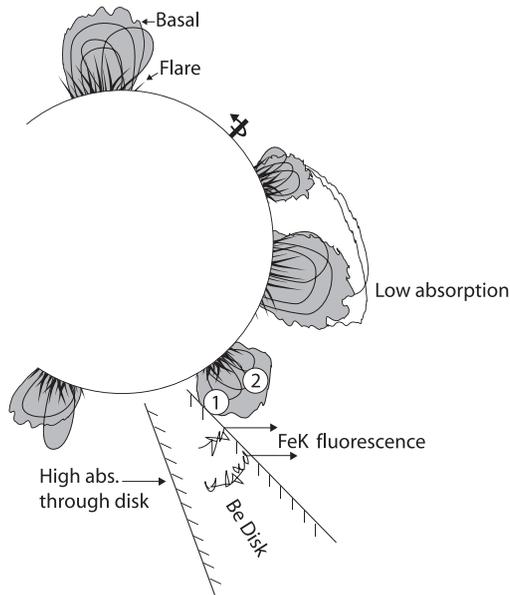
FIG. 4.—Sketch of a cross-section of γ Cas inclined at 45° to the observer at right. In our picture (see also SRC98) the star's surface is populated by small X-ray flare centers, which fill canopies within magnetic loops as they explode. The observed hard X-rays are produced in both regions. The Be (decretion) disk is in the star's equatorial plane and absorbs all the soft X-rays but rather little of the hard X-rays and a fraction of the hard flux emitted from the canopies viewed behind the disk at lower left. The disk is also the presumed site of Fe and Si K fluorescence photons, which are end products of photo-ionization from very hard continuum X-ray photons. The symbols "1" and "2" correspond to sites in a typical basal flux–emitting canopy where soft X-rays are generated either from canopy-cloud collisions with the disk (case 1) or cooling within the canopies (case 2).

see whether this absorption edge is present in the data by extracting two small spectral windows immediately below and above the edge at 23.3–23.8 and 22.4–22.9 Å. There are no known strong line emissions in these two wavelength intervals. The flux ratio of these two windows in the HEGS data is $F(23.3-23.8)/F(22.4-22.9) = 0.94 \pm 0.22$, while the corresponding ratio is higher, equaling 2.8, for model M2. However, since the quoted uncertainties account only for finite photon statistics, we feel it is premature to rule out the possible existence of the O I edge. We are planning to search for this feature in upcoming *XMM-Newton* observations.

To summarize this analysis, although it is hard to quantify the exact uncertainties on each parameter in a complex thermal model, we have found (1) two separate column densities are required for the hot component, (2) several warm-temperature components or a continuous temperature distribution of warm plasma with several peaks is required in addition to the hot component, and (3) the hot component has a significantly lower Fe abundance than the warm components. These conclusions are robust, as indicated by the inability of alternative models to provide good global fits to the data.

3.5. *Comparison of X-Ray– and Ultraviolet-derived Column Densities*

The analysis in the previous section established that both the hot and warm X-ray components are absorbed by a gas with a column density of 3×10^{21} atoms cm^{-2}. This value, which is again partly a consequence of our assuming a temperature of 11–12 keV from the literature, is consistent

with the results of previous X-ray studies, which find column densities in the range $10^{21}-10^{22}$ atoms cm^{-2} toward γ Cas (see Table 2). Most of these previous studies attribute the absorption to the interstellar medium (ISM). For the *RXTE* and *Tenma* studies, the instrumental flux calibrations below 2–3 keV were not as well determined, so the rather high column density estimates derived in these cases are suspect. The remaining estimates cluster tightly at $(1.5-1.6) \times 10^{21}$ atoms cm^{-2}. In contrast to the X-ray results, the column densities derived from UV studies of ISM resonance and Lyα lines show much lower values. In the case of γ Cas, the broad absorption core of Lyα is produced by an ISM column density of 1.4×10^{20} atoms cm^{-2} in *Copernicus* spectra (Bohlin, Savage, & Drake 1978). Various *IUE* studies (e.g., van Steenberg & Shull 1985, 1988, 2×10^{20} atoms cm^{-2}; Diplas & Savage 1994, 1.5×10^{20} atoms cm^{-2}) show an excellent consistency. Moreover, the resonance line results for five metallic ions, relative to the expected depletions in the ISM of metal, also bear out the $N_{\rm H}$ result determined from the Lyα line core measurement (van Steenberg & Shull 1988). To summarize, the UV metal and hydrogen lines toward γ Cas are all low and show inter alia agreement. In contrast, X-ray spectra lead to column densities some 10 times higher than the UV results, according to the wavelength attenuation of the soft X-ray continuum. The excess absorption in the X-ray case (the 10^{21} atoms cm^{-2} component) can be easily explained by there being much more cold gas near the star than ISM material along the line of sight to it.

3.6. *Analysis of Diagnostics of Volume Density*

Our spectrum reveals density diagnostics, including partial sets of two "*rif*" triplets of He-like Si XIII (6.6–6.7 Å), Ne IX (13.4–13.5 Å), and O VII (21.6–22.1 Å), as well as the 17.05 and 17.10 Å lines from the strong $2p^6 \rightarrow 2p^5 3s$ transitions of Fe XVII. The forbidden *f* component of O VII is too weak to be detected in our spectrum. Likewise, for Si XIII, the inter-combinational (*i*) component is not visible, and the *f*-component detection is doubtful. The latter components lie on the Si edge of the detector responses, so the $I(f)/I(i)$ ratio is indefinite and can add no information. For Ne IX and O VII it is more apparent that the ratio $I(i) + I(f)/I(r) \leq 1$ and that $I(f)/I(i) \simeq 0$. (The former ratio is visible for Si XIII as well.) The first ratio argues that the plasma is collisionally dominated, while the second indicates that the forbidden component is quenched by either collisions or photoexcitations. The colli-sional interpretation for the f/i ratio would set the plasma density at $\sim 3 \times 10^{11}$ and $\geq 3 \times 10^{10}$ cm^{-3} for the Ne IX and O VIII ions, respectively. One can perhaps discriminate between the collisional and photoexcitation options for γ Cas by com-paring the photoexcitation and decay rates of the $2\,^3S \rightarrow 2\,^3P$ transition appropriate for a 1000 Å radiation field of a B0.5 Ve star. Scaling from rates given by Kahn & Leutenegger (2001), one finds that radiative dominance requires only that the Be star be nearer to the irradiated plasma than $10R_*$ and $40R_*$, re-spectively. In the picture of X-rays being produced by an ac-creting white dwarf, the corresponding limits would mean a similar dilution factor of 10^{-2}–10^{-3}. In the Be X-ray paradigm, the hot sources are no further from the star than the magnetic corotation radius, which is probably less than one stellar radius. Since the photoexcitation diagnostics turn out to be only weak constraints and because both the density and irradiation routes are available to quench the forbidden components, little new information is actually gained from these triplets.

A final estimate of the densities can be obtained from the dimensionless ionization parameter $\Xi = L_X/(4\pi r^2 c_s P)$ (e.g., Nayakshin, Kazanas, & Kallman 2000) and the fact that collisional processes dominate whenever $\Xi < 1$. Here L_X is the luminosity of the hot X-ray flux, r the distance to gas particles illuminated by these sources, P the local gas pressure, and c_s the speed of sound. Thus, a lower limit on the gas density is obtained by assuming $\Xi = 1$ and solving for the pressure, which can be converted to density by selecting an appropriate temperature. As an example, we consider the situation in which hot X-ray sources strongly illuminate a nearby reservoir of cold gas, such as the Be disk. We assume that the disk is at least as far away from the illuminating sources as the size of the hot X-ray regions themselves ($\sim 10^{11}$ cm, estimated by SRC98). We further assume a temperature of 10^6 K for the average warm component. From these values, we obtain the limit $n_H > 10^9$ cm^{-3} for the gas density of the warm component plasma.

4. DISCUSSION

In this section we acknowledge that while an X-ray spectrum can provide a glimpse of the physical conditions in the hot-plasma sites where the flux is produced, it is not likely to point the way to a truly unique model or geometry of these regions. Nonetheless, we do believe that there are telltale hints of their proximity to the Be star. In this section we first examine the Be star model, paying particular attention to our column density estimates and to the role of cold gas in providing fluorescence and attenuation of the spectrum. The influence and hence proximity of this material can provide evidence pertinent to this picture that cannot be obtained from other kinds of observations. We then compare the X-ray spectral properties of γ Cas with those of known binary systems containing an active white dwarf companion.

4.1. Relationships among the X-Ray–Emitting Components

4.1.1. Fe Fluorescence: "Cold Matter"

Our measured equivalent widths of the Fe and Si K fluorescence features are -19 mÅ and -5 Å, respectively. The presence of these lines indicates that substantial "cold" gas is present along the lines of sight to the hot X-ray emission sites. Although modeling the Fe fluorescence feature is quite complicated and depends on details of the temperature of disk particles and disk geometry, we can get a rough estimate of the formation parameters for this line by adopting a simple model, which is sketched in Figure 4. Consider the fluorescence within a cold plane-parallel slab illuminated by numerous hard X-ray sources placed just behind and in front of it. If the slab is optically thin to X-ray photons with wavelengths below 1.94 Å, some of the photons will photoionize the K shell of Fe atoms, and some $\frac{1}{3}$ of them will emit fluorescence photons with wavelengths near 1.94 Å (Liedahl 1998). Because fluorescence is an isotropic process, it produces essentially the same feature whether the optically thin slab is illuminated from the front or back by the hard X-ray sources. Now stipulate further that the slab has a solar composition and an arbitrary column thickness of 10^{23} atoms cm^{-2}. Its X-ray spectrum should also be flat in the 1.3–1.94 Å region regions of the Fe K continua. Under these assumptions Kallman (1991) has computed an equivalent width of -69 mÅ for the 1.94 Å fluorescence feature. The geometry just described provides a reasonable approximation of the X-ray sites and disk thought to be associated with γ Cas. The value of 10^{23} atoms cm^{-2} that we

have used here and elsewhere in this paper is taken from the predicted (vertical) disk column density of Millar & Marlborough (1998, hereafter MM98) for the γ Cas disk. Moreover, we have already found that it is a reasonable estimate of the column density according to the long-wavelength attenuation in the HETGS spectrum. In the picture we have described, hot X-ray sites are evenly distributed over the surface of the Be star and illuminate the Be disk. Fe continuum photons from these sites are converted by Fe atoms in the Be disk to ≈ 1.94 Å photons by the fluorescence process and are emitted isotropically. Since the sites reside near the star, no more than half the outward-directed flux can illuminate the disk. Thus, in this rough approximation, we might expect the equivalent width of the Fe fluorescence line to be about $-69/2 = -35$ mÅ. This figure agrees reasonably well with the observed value of -19 mÅ. The discrepancy of a factor of 2 in this estimate might be attributable to the actual decreasing continuum slope shortward of the K feature or to an oversimplified distribution of the hot-plasma sources. Considering the uncertainties in our picture, we regard the observed strength of the fluorescence feature to be consistent with the presence of intervening disk particles having the column density estimated by MM98.

4.1.2. Origin of the Two Absorption Systems

The two-column absorption model required for the hot-emission component in § 3.4 is an expected outcome if the emission sites themselves are sprinkled closely around the Be star such that some fraction of them are behind the disk but still in our line of sight. Various correlations of X-ray fluxes with UV diagnostics indicate that the flare and basal components are probably formed at or at most within a few tenths of a radius of the star's surface (see SRC98; SRH98; Smith & Robinson 1999). Referring to the sketch in Figure 4, if the X-ray–active sites are distributed uniformly over the star and close to the surface, the ratio of the sites in front of the Be disk to those behind it will be $\simeq 0.25$. We used this geometric visualization in § 3.4, as well as the MM98 disk thickness for the "high" column density, to arrive at the ratio of 2 absorption columns of the hot subcomponents for our models M2 and M3.

There are two possible CS gas structures near the Be star that could be responsible for the "low" column density (3×10^{21} atoms cm^{-2}) required from our modeling of the soft X-ray continuum. The first is any intermediate-latitude gas residing near the top and bottom boundaries of the Be disk, while the second is the intermediate-latitude wind. In the first instance, soft X-rays can be created and partially absorbed within the outer boundaries of the disk. However, this requires a fine-tuning of the placement of the emission volumes within the upper and lower boundaries of the disk, which we deem unsatisfactory. The possibility of wind absorption seems easier to accept. For example, as CSR00 have discussed, the wind column density of γ Cas lies in the range 10^{21}–10^{22} cm^{-2}. Since this agrees very well with our result for N_H in Table 3, the wind can be regarded as the leading contender for the source of the low column component of X-ray absorption.

4.1.3. Warm X-Ray–Emitting Components

The rather different Fe abundances of the hot and warm plasmas, as well as the likely break in the DEM between these temperatures, indicates that the corresponding emission volumes are not cospatial. The combination of a 12 keV

component with one or more components with temperatures extending down to 0.1 keV is very unusual in a B star. This leads to the question of whether the hot- and warm-component volumes are in close proximity and indeed might be causally related. It is possible, for example, that the hot and warm components are different manifestations of the same driving process, such as the magnetic field reconnections, which are thought to create the flarelike shots.

Alternatively, we note that the hot plasma has 7–10 times the emission measure of the warm plasma and also a higher energy per particle. Since the thermal energy within hot plasma is as much as 50 times the energy within the warm X-ray–emitting regions, it is feasible energetically that the warm plasma is heated by processes occurring within the hot-plasma regions. An obvious possibility is that warm component arises from the photoionization of nearby cold gas by the hot X-ray flux. On the other hand, we have already all but ruled out this possibility because, except for the fluorescence features, the prevailing diagnostics in the spectrum clearly favor a collisional source of heating. Such heating can arise in a number of ways. The first, case 1, is that *the hot component heats the preexisting gas disk by colliding with it.* To see how this might happen, recall that SRC98 found from plasma-cooling arguments that the heated plasma from initial flaring on the stellar surface expands rapidly and without much energy loss, so that it is free to collide with preexisting stationary gas in, for example, the Be disk. A second possibility, case 2, is that the warm components are simply *the result of radiative cooling of the hot plasma.* Cooling curves of hot plasma (e.g., Cox 2000) show the presence of plateaus or minima in the cooling rate at temperatures of $\simeq 0.1$, 0.3–0.4, and 2–3 keV. These are values very similar to those of components 2–4 in our models (and also temperatures found for the B0.2 V star τ Sco, discussed) and suggest that the triple-peaked DEM of these components could be a consequence of plasma accumulating at these temperatures as it cools from its initial high value of 10^+ keV. However, this picture presents the difficulty of explaining how the Fe abundance in the very same plasma could increase to the solar value as it cools. We return to this question below.

Case 2 suggests that the warm-component plasma resides in corotating volumes attached to the star's surface (see SRC98; SRH99), while case 1 favors the inner regions of the Be disk, which have a Keplerian rate. In the range of interest, within 1 stellar radius of the surface, the two velocities are rather similar. Consider that the rotational velocity $v \sin i$ of γ Cas has been variously measured in the range 230–380 km s^{-1} (Slettebak 1982; Harmanec 2002), and larger velocity broadenings cannot reasonably arise from either the photosphere or from a disk in Keplerian orbit. Then the observed X-ray line broadening of 478 km s^{-1} is consistent with material forced into corotation at fairly low altitudes over the Be star's surface (case 2). However, this broadening is also consistent with the orbital velocity of the inner disk, the environment we associate with case 1, for which broadening of high-level hydrogen lines has been found up to 550 km s^{-1} (Hony et al. 2000). Thus, the broadening of the X-ray lines cannot be used to discriminate between the cooling residue and colliding ejecta pictures.

Analogs in other B stars (τ Scorpii).—We can also consider alternate causes for the production of warm-component X-rays in an ostensibly single early B-type main-sequence star. Possibly the best such case is the B0.2 V spectral standard, τ Sco. The UV spectrum of this star is anomalous in that it exhibits P Cygni profiles in its resonance O VI, N V, and C IV lines. The absorption components of these profiles are abnormally broad

while the emission components are significantly redshifted. Analyses of *ASCA, Chandra* HEG, and *XMM* RGS spectra (Cohen, Cassinelli, & Waldron 1997b; Cohen et al. 2003; Mewe et al. 2003) demonstrate that the X-ray emissions have a complicated emission measure that extends to high temperatures. The high-resolution studies showed that the X-ray emission measure is composed of as many as three components with kT values centered near ≥ 2.5, 0.7, and 0.1 keV. According to predictions of standard wind theory, the high temperatures corresponding to the first two components are unlikely to be attained by wind shocks. However, in the Howk et al. (2000) scenario these emissions arise from failed ejecta returning violently to the star's surface. Because the spectrum reveals the presence of the Lyα 34 Å line of C VI (Mewe et al. 2003), for which the ionization potential is within a factor of 3 or 4 of O VI, it does seem reasonable to us to assume a connection between the soft X-ray and UV attributes. This leads to the question, Can the warm kT_2 and kT_3 components in γ Cas be identified with the 0.7 and 0.1 keV components in τ Sco? We believe the answer to this question is no. According to Cohen et al. and Mewe et al., the ≥ 2.5 and 0.7 keV component emissions are likely to arise from the peculiar properties of this star's wind, such as from returning clumps of a partially stalled wind. This can be explained by ~ 1000 infalling clumps, which would represent a substantial fraction of the mass in the star's exosphere at any one time (Mewe et al. 2003). Yet, in our view it does not seem likely that this scenario can occur in γ Cas's wind.[2] Consider that its wind is much weaker than τ Sco's, either as measured by its mass-loss rate (3.1×10^{-8} vs. $\sim 1 \times 10^{-8}$ $M_\odot$; Howk et al. 2000; Waters et al. 1987) or its terminal velocity (-2400 vs. -1800 km s^{-1}; Howk et al. 2000; Smith & Robinson 1999). In addition, even though the wind is weaker in γ Cas, the emission measures of its components 2 and 3 are nearly 10 times larger than the components with these approximate temperatures in τ Sco. There is no indication of emission or redshifts in the absorptions of the N V and C IV line profiles of γ Cas, and an archival *Far-Ultraviolet Spectroscopic Explorer* spectrum taken in the scattered light of γ Cas shows no emission or absorption components of the O VI lines. Thus, it seems difficult to reconcile the hypotheses that the UV line anomalies are related to the X-ray emission and that these X-ray components are caused by a common mechanism in the two stars. In sum, it appears that warm components in the γ Cas X-ray spectrum are unique for this star. Moreover, we do not have a firm picture of the warm-site geometry.

We turn next to alternative origins for the kT_4 component. In their *ROSAT* PSPC survey of 27 normal B stars in the solar neighborhood, Cohen, Cassinelli, & MacFarlane (1997a) found that the soft X-ray emissions of early B stars are consistent with a wind shock origin. The observations show temperatures of $\simeq 1$ MK (0.085 keV) and typical emission measures of $\simeq 10^{54}$ cm^{-3}. Although this temperature is consistent with our fourth component, the typical emission measure in field B stars is a factor of 4 lower than we found for model M2. Even in τ Sco, with its dramatic wind signatures in the UV resonance lines, the emission measure is a factor of

---

[2] The following discussion presupposes that the wind of γ Cas is similar to those of other Be stars for its spectral type, as indeed previous studies have suggested (e.g., Henrichs et al. 1983; Doazan et al. 1987; Grady, Bjorkman, & Snow 1987). It is possible that τ Sco's is observed from a polar aspect, which might explain its anomalous strength for a B0 star. Thus, while the emission measures of γ Cas's warm subcomponents are puzzling on one hand, it is actually the strength of τ Sco's wind that remains the long-standing enigma.

2 below our value of EM_4. An additional fact to keep in mind is that the wind signatures in the UV resonance lines indicate that γ Cas's wind characteristics are consistent with those of other B0.5e main-sequence stars (see Henrichs et al. 1983; CSR00). From these considerations, it seems that at most only part of the kT_4 component can arise from processes associated with a B star wind. We hope that a planned *XMM* RGS spectrum will shed light on the origin of the cooler components, particularly kT_4.

4.1.4. Fe *Anomaly in the Hot-Plasma Component*

In our best models we find the Fe abundance to be approximately 0.22 ± 0.05 solar, yet the Fe and other metallic abundances for the warm component's X-ray emissions are close to the solar value. By comparison, the Fe abundance determined for B stars from *ASCA, Chandra,* and *XMM* observations are also nearly solar (0.6–1.0; e.g., Kitamoto et al. 2000). These values are in agreement with the general slight underabundance of about 30% for the local interstellar medium and photospheric abundances for galactic OB stars. The data on Fe abundances in X-ray–emitting plasmas associated with somewhat abnormal hot stars are still fragmentary. However, if the example of the Wolf-Rayet star WR 25, with possible colliding winds, is typical, then the Fe abundance does not differ from main-sequence values. Moreover, results for the same stars observed with the HETGS and *XMM* or *ASCA,* including γ Cas, are the same within expected errors. The Fe abundance in the hot-plasma component is certainly lower than values found in other upper main-sequence stars, and we now discuss several possible causes that can lead to this anomaly.

Oversimplified modeling.—A number of simplifying assumptions were made in our global-fitting analysis that are known to affect Fe abundances estimates. These fall into two general categories, nonequilibrium physics and a broad DEM with an arbitrarily high temperature limit. The general problem in these cases is that the temperatures derived from the continuum shape and the Fe ionization often do not agree. Transient ionization can occur in rapidly evolving rarefied plasmas if the dynamical timescale is shorter than the recombination timescale. We do not expect transient states to occur for the hot plasma associated with γ Cas because this component should have a relatively high density (10^{11}–10^{13} cm^{-3}), according to the analysis of SRC98.

The apparent continuum temperature can also be misdetermined by relying on an oversimplified high-energy model, e.g., by failing to include a needed second high-energy component and/or (as for some cataclysmic variables [CVs]) by reflection of hard X-rays from the nearby star. This problem could be important for our case if the temperature measured from the Fe line ratio were at the low end of a continuous DEM extending to high temperatures. The continuum at short wavelengths would then be enhanced by contributions from higher temperatures and would dilute the Fe line strengths. In actuality, the spectrophotometry of the *RXTE* and *BeppoSAX* instruments gives no hint of a flux excess at high energies. The addition of an ultrahigh temperature component is also contradicted by the agreement of the temperatures inferred from the short-wavelength *ratio* of the Fe K line strengths.

Anisotropic scattering.—For special geometries in optical plasmas anisotropic scattering can deflect Fe line photons from the observer's line of sight and modify its equivalent width. However, the circumstances surrounding X-ray flares suggests that this is unlikely. Flares occur continually and are likely to be distributed roughly evenly around the star's azimuthal sectors. The strength of the K fluorescence and the fraction of low-to-high absorption columns of the hot component are both consistent with the more or less isotropic sprinkling of these sources around the star and offer no special geometry that could remove photons from the line of sight. Even if a special configuration offered itself at some phase, it is doubtful that it would remain for many viewing angles associated with our 53 ks integration.

Donor star has a low Fe.—The determination of Fe abundances in stars with hard X-ray spectra, such as CVs, is fraught with perils caused by the reflectivity of the hard X-rays from the star's surface and the variable K-absorption edge of Fe. Most available Fe abundance studies from X-ray lines suggest that they lie in a range extending from about 0.2 to, more typically, fully solar (Ezuka & Ishida 1999). Since the abundance we find for γ Cas is at best at the lower boundary of this range, it is not reminiscent of chemical processing in CV material, which may be due to low abundances in the secondary donor star. Because of the wide separation between the component stars of the γ Cas binary system (Miroshnichenko et al. 2002), it is unlikely that the surface of the primary would be contaminated by material from a metal-deficient secondary.

Donor is the Be star.—If the Fe-deficient plasma is provided by the Be star with assumed normal abundances, then the low abundances might be somehow caused by processes associated with the high temperature conditions. The notion that the low Fe abundance becomes normal when the plasma cools, as in case 2 above, implies that surplus Fe atoms are somehow created and restored to the gas as a part of the cooling process, an ad hoc proposition. The alternative is that the high temperatures somehow promote the Fe anomaly. This concept is reminiscent of the famous first ionization potential (FIP) effect in which elements that have a FIP below 10 keV observed in the slow solar wind, flares, and comparatively small-scale structures in the solar corona all exhibit abundances enhanced by a factor of 3–4 times relative to those elements with a FIP above this value (Feldman 1992) in the slow wind, flares, and comparatively small-scale coronal magnetic structures. The exact process for this effect is still unknown but probably involves incomplete Coulombic coupling between ions due to a combination of gravitational settling and particle-magnetic interactions occurring in intermediate-density plasma (see Raymond 1999)

An inverse FIP effect, in which the low-FIP elements such as Fe are deficient and the high-FIP ones are approximately normal, has been by now widely observed in the high-resolution EUV and/or X-ray spectra associated with the coronae of the active primaries of RS CVn binaries (e.g., Brinkman et al. 2001; Drake et al. 2001; Audard et al. 2003). For example, the Fe abundance in the corona of the primary of the prototypical system HR 1099, as derived from its *XMM* RGS spectrum, is only 0.25 solar (Brinkman et al. 2001). Güdel et al. (2003) have suggested that the inverse FIP effect is due to high-energy electron beams (as evidenced by their observed radio gyrosynchronous radio emission), which propagate along magnetic lines into the star's chromosphere. Low-FIP ions are prevented from escaping into the corona by the strong downward-directed electric field created by this beam. This mechanism squares seemingly perfectly with the picture suggested by Robinson & Smith (2000) in which X-ray flares of γ Cas are produced as a consequence of accelerated beams into its upper atmosphere from field stresses introduced between the rotation rates of the Be star and its Keplerian disk.

There may be other circumstantial links between the inverse FIP effect and a beam flare mechanism. According to Güdel et al. (2003), the one other star known to harbor magnetic corotating clouds, the active K dwarf AB Dor, shows X-ray flaring and an inverse FIP effect. These authors have noted that the strength of this effect moderates for Fe during flaring events in this star, and this also seems to be the case for HR 1099 (Audard et al. 2001). The moderation of this effect is indeed predicted during strong flaring by the Güdel et al. mechanism.

As a variant of the "classical" FIP interpretation, S. R. Cranmer (2003, private communication) has also pointed out that *SOHO* satellite observations of the solar corona have indicated a classical FIP-like pattern of abundances for gas located in the middle regions of large solar coronal structures called helmet streamers. In these central regions matter seems to be the most stable and thus least able to be completely mixed (Raymond 1999). The abundance pattern introduced is similar to the classical FIP effect itself, except that a metal deficiency bias is introduced such that the low-FIP ions such as Fe are deficient by a factor of 3 and the high-FIP ions, by a factor of 10. Interestingly, complete stability in atmosphere is apparently not needed for this anomaly to develop. In the solar case, mass circulation caused by chromospheric spicules is 100 times greater than net outflow assumed in chromospheric diffusion models (Athay 1976). An additional consideration is that total stability in the solar corona would mean that gravitational diffusion alone would impose abundance gradients orders of magnitude greater than is observed, so some type of mixing seems actually to be required, by either kinetic or magnetic processes (Raymond 1999). In this connection, we note that on γ Cas the role of surface flares, which are confined to small volumes and which occur over timescales much shorter than the gravitational settling timescale, may be equally irrelevant to any stability requirements as chromospheric spicules are in the solar case.

Given the commonality of some form of FIP effect in active cool stars, it seems that Fe deficiency is becoming almost an expected hallmark of active magnetic stars and indeed may even be linked to particle beams needed for the production of X-ray flares. Thus, the existence of this effect in γ Cas is additional circumstantial evidence that the hard X-rays are produced as a by-product of magnetic field stresses associated with the Be star and its disk. We should also note that if the FIP effect is the correct explanation for the Fe deficiency it strengthens the argument that the warm plasma comes from a reservoir of material separate from the hot component (case 1).

4.2. *Comparisons with Cataclysmic Variable Spectra*

The suggestion has been made recently (Kubo et al. 1998; Apparao 2002) and countered (Robinson & Smith 2000) that an active Be–white dwarf system is responsible for the hard and luminous X-ray flux of γ Cas. Historically, one of the chief reasons for this suggestion has been the detection of moderate-strength H- and He-like Fe lines in the spectrum, indicating emission from a hot optically thin gas (Murakami et al. 1986). In the general binary accretion picture (and considering more carefully the likely evolution of the members of this binary), a young γ Cas binary could evolve to become a Be-NS system. However, such binaries exhibit nonthermal spectra and weak Fe K lines. Moreover, Be-NS systems generally have eccentric orbits and also have a strong likelihood of emitting X-ray pulses, for which extensive searches have proved negative.

Let us consider instead the accreting white dwarf picture, e.g., as suggested by Kubo et al. (1998). Recently published *Chandra* spectra of several CVs (notably U Gem and TX Hya) in their quiescent states exhibit both similarities and dissimilarities to the γ Cas spectrum. The X-ray continuum of these objects is consistent with a (generally) optically thin two-temperature model. The hotter and dominant component typically has a value $kT \approx 15$–80 keV (see Szkody et al. 2002; Mauche 2002; Mukai et al. 2003). The second "cool" component (0.1–2 keV) is most easily observed in EUV wavelengths. In magnetic CVs, Roche-overflowing mass is channeled to the magnetic poles of the white dwarf, causing an accelerated column flow to shock as it impacts on the star's surface (e.g., Warner 1995). In nonmagnetic stars undisrupted accretion disks extend to the star's surface, and turbulent energy in the shear layer thermalizes and radiates X-rays (Patterson & Raymond 1985). In both cases the emergent flux distribution results from a broad distribution of temperatures radiating from the hard X-ray to EUV spectral domains. Because these components roughly resemble the multiple components we have identified in our DEM analysis, there is some resemblance between the spectra of γ Cas and the CVs, so we examine this further.

Mukai et al. (2003) has argued for a dichotomous classification of CVs on the basis of the spectra of the seven of them observed to date by *Chandra*. One of these subgroups consists of white dwarfs with low or undetectable magnetic fields and/or low specific mass transfer rates. The second subgroup, having much stronger magnetic fields, consists of intermediate polars with associated high rate and channeled mass transfers, and their spectral properties are consistent only with photoionization-dominated processes. These authors point out that the *ASCA* and *Chandra* spectra of the nonmagnetic group exhibit emission primarily in lines of Fe L-shell ions (Fe XVII–XXIV), as well as lines of H-like S, Si, Mg, Ne, O, and N. The kinematic properties of this group are also similar to those inferred for γ Cas. For example, their lines indicate a rest velocity and broadenings of 200–550 km s^{-1}. Moreover, spectra of well-studied systems such as U Gem and TX Hya also show density-sensitive diagnostics that indicate $n_e \geq 10^{14}$ cm^{-3} and/or small dilution factors for EUV/UV radiation. However, the nonmagnetic spectra exhibit neither a substantial K fluorescence strength nor attenuated long-wavelength continua. Spectra of the second, magnetic polar group stand in marked contrast to spectra of either γ Cas or the nonmagnetic group. For example, their hard continua are best fitted with a nonthermal model. Their spectra also have weak or undetectable lines of Fe L-shell ions, as well as only weak lines of the H-like ions. In short, the γ Cas spectrum cannot be reconciled with the Mukai et al. dichotomy since this spectrum shows hybrid evidence of dominant collisional processes and yet also exhibits a moderate-strength Fe fluorescence feature. The γ Cas spectrum is also unique in requiring two separate Fe abundances and absorption systems.

5. CONCLUSIONS

Our previous series of papers discussed in some detail the temporal variations of the X-rays of γ Cas and their correlations with various optical and UV spectral indicators and broadband fluxes (see Smith & Robinson 2003). In this study we have found that the spectral features of this star are eclectic and suggest at least three different X-ray generation environments. Taken together, the spectral signatures appear to be just as unique as its temporal and colorimetric properties. They may be summarized as follows:

First, the HEG/MEG emission is produced by several plasma components, each of which seems to be thermal and collisionally dominated. The primary "hot" component has a temperature of 10–12 keV and a distinctly subsolar Fe abundance. This component is responsible for the emission of both the short-wavelength continuum and the Fe xxv and xxvi lines. A subcomponent of the hot plasma, about 3 times smaller in volume than the primary subcomponent, is heavily attenuated at long wavelengths by gas having a column density of $\approx 10^{23}$ cm^{-2}. Some 10%–14% of the total emission measure is produced by a "warm" component. The DEM of this warm component may be continuous over the range of about 0.1–3 keV (though it seems to require definite peaks), or it may contain the three discrete components at $kT_2 = 3$, $kT_3 = 0.37$, and $kT_4 = 0.15$.

Second, although the different Fe abundances for the warm and hot emission sites argue that the emissions are not cospatial, it is doubtful that they are completely unrelated. For one thing, a "warm"-component EM of nearly 10^{55} cm^{-3} seems to be atypical among B stars. It is more natural to attribute it to the (also unique) hot component, for example, by shock heating as the hot sites impact on the edges of the Be disk. Alternatively, the warm and hot components could be somehow produced by a common external mechanism, such as through heating associated with the magnetic reconnections responsible for the hot flare and canopy subcomponents. However, since these are all speculations, we still have no good sense of the geometry or of the cause(s) of the warm components.

Third, the X-rays are absorbed by cool material located in at least two types of structures. The first type affects both the warm and most of the hot X-ray emission and has a column density of $(1–3) \times 10^{21}$ atoms cm^{-2}. This is most probably the stellar wind or outer regions of the decretion disk. The second structure has a column density of $\sim 10^{23}$ atoms cm^{-2} and is detected primarily by its effects on a fraction of the hot X-ray component. Some emission from the warm component is probably also affected by this gas. However, the column mass is so large that this emission is completely absorbed. This gas is probably also the source of the Fe and Si K fluorescence features. We have identified this absorbing gas as the dense portion of the circumstellar disk and as such it is in close proximity to the sites of hard X-ray production.

Fourth, we have emphasized the peculiar Fe deficiency in the hot-plasma component, whereas the warm components show nearly solar metallic abundances. So far as we are aware, this is a unique attribute of an X-ray spectrum of a hot star.

Thus, if the Fe abundance anomaly turns out to arise from a FIP-like effect, it would be the first discovery in a hot star (for example, it is not present in τ Sco; Mewe et al. 2003). The effect itself might then become a proxy in stars for which detection of Zeeman splitting is often impossible. If these ideas are approximately correct, one might expect to see deficiencies of Fe and other low-FIP elements in other hot astronomical venues.

We count three attributes of the spectrum that argue for the association of the X-rays with either the Be star or its disk: (1) the long-wavelength attenuation of fluxes, (2) the generation of moderate-strength Fe and Si K fluorescence features, and (3) the Fe abundance deficiency, which we suggest is associated with the FIP effect. In contrast, these attributes are hard to reconcile with high-resolution spectra of the well-observed CVs to date. Moreover, the spectral characteristics of γ Cas do not fit into the context of OB star behavior either. In a preliminary survey of line widths among galactic O and early B stars, Cohen et al. (2003) found that line widths decrease with spectral type from large values down to ~ 250 km s^{-1} at B0.2. Thus, viewed in the context of X-ray generation in a magnetic environment, the larger line widths for γ Cas are unexpected. Neither are the line profiles consistent with magnetic confinement or high-velocity outflow. Alternatively, although it is not a unique interpretation, we have suggested that the line broadening is caused by the corotation of circumstellar material or the Keplerian velocities of the inner Be disk. It is perhaps pertinent to point out that in the magnetic dynamo model of RSH02, it is just those conditions within a stellar radius where stresses might be expected to lead to magnetic dissipation and the production of particle beams and X-rays.

REFERENCES

Apparao, K. M. V. 2002, A&A, 382, 554
Athay, R. G. 1976, The Solar Chromosphere and Corona: Quiet Sun (Dordrecht: Reidel), 36
Audard, M., Güdel, M., & Mewe, R. 2001, A&A, 365, L318
Audard, M., et al. 2003, A&A, 398, 1137
Bohlin, R. C., Savage, B. D., & Drake, J. F. 1978, ApJ, 224, 132
Brinkman, A., et al. 2001, A&A, 365, L324
Cohen, D. H., Cassinelli, J. P., & MacFarlane, J. J. 1997a, ApJ, 487, 867
Cohen, D. H., Cassinelli, J. P., & Waldron, W. L. 1997b, ApJ, 488, 397
Cohen, D. H., et al. 2003, ApJ, 586, 495
Cox, A. N. 2000, Allen's Astrophysical Quantities (New York: Springer), 193
Cranmer, S. R., Smith, M. A., & Robinson, R. D. 2000, ApJ, 537, 433 (CSR00)
Diplas, A., & Savage, B. 1994, ApJS, 93, 211
Doazan, V., Rusconi, L., Sedmak, G., Thomas, R. N., & Bourdonneau, G. 1987, A&A, 182, L25
Drake, J. J., et al. 2001, ApJ, 548, L81
European Space Agency. 1997, The Hipparcos and Tycho Catalogues (ESA SP-1200; Noordwijk: ESA)
Ezuka, H., & Ishida, M. 1999, ApJS, 120, 277

Feldman, U. 1992, Phys. Scr., 46, 202
Grady, C. A., Bjorkman, K. S., & Snow, T. P. 1987, ApJ, 320, 376
Güdel, M., et al. 2003, in ASP Conf. Ser. 277, Stellar Coronae in the Chandra and XMM-Newton Era, ed. F. Favata & J. Drake (San Francisco: ASP), 497
Harmanec, P. 2002, in ASP Conf Ser. 279, Exotic Stars, ed. C. Tout & W. Van Hamme (San Francisco: ASP), 221
Harmanec, P., et al. 2000, A&A, 364, L85
Henrichs, H. F., Hammerschlag-Hensberge, G., Howarth, I. D., & Barr, P. 1983, ApJ, 268, 807
Hony, S., et al. 2000, A&A, 355, 187
Howk, J. C., Cassinelli, J. P., Bjorkman, J. E., & Lamers, H. J. 2000, ApJ, 534, 348
Kahn, S. M., & Leutenegger, M. A. 2001, A&A, 365, L312
Kallman, T. R. 1991, in Fe Line Diagnostics in X-Ray Sources, ed. A. Treves, G. Perola, & L. Stella (Berlin: Springer), 87
Kinkhabwala, A., et al. 2002, ApJ, 575, 732
Kitamoto, S., Tanaka, S., Susuki, T., Torii, K., Corcoran, M., & Waldron, W. 2000, Adv. Space Res., 25, 527
Kubo, S., Murakami, T., Ishida, M., & Corbet, R. H. D. 1998, PASJ, 50, 417

Liedahl, D. 1998, in X-Ray Spectroscopy in Astrophysics, ed. J. van Paradijn & J. Bleeker (Springer: Amsterdam), 189

Mauche, C. W. 2002, in ASP Conf. Ser. 261, The Physics of Cataclysmic Variables, ed. B. Gansicke, K. Beuermann, & K. Reinsch (San Francisco: ASP), 113

Mewe, R., Raassen, A. J., Cassinelli, J. P., van der Hucht, K. A., Miller, N. A., & Güdel, M. 2003, A&A, 398, 203

Millar, C., & Marlborough, J. M. 1998, ApJ, 494, 715 (MM98)

Miroshnichenko, A., S., Bjorkman, K. S., & Krugov, V. D. 2002, PASP, 114, 1226

Mukai, K., Kinkhabwala, A., Peterson, J. R., Kahn, S. M., & Paerels, F. 2003, ApJ, 586, L77

Murakami, T., Koyama, K., Inoue, H., & Agrawal, P. 1986, ApJ, 310, L31

Nayakshin, S., Kazanas, D., & Kallman, T. R. 2000, ApJ, 537, 833

Owens, A., Oosterbroek, T., Parmar, A. N., Schulz, R., Stëwe, J. A., & Haberl, F. 1999, A&A, 348, 170

Parmar, A., Israel, G., Stella, L., & White, N. 1993, A&A, 275, 227

Patterson, J., & Raymond, J. C. 1985, ApJ, 292, 535

Quirrenbach, A., et al. 1997, ApJ, 479, 477

Raymond, J. C. 1999, Space Sci. Rev., 87, 55

Robinson, R. D., & Smith, M. A. 2000, ApJ, 540, 474

Robinson, R. D., Smith, M. A., & Henry, G. W. 2002, ApJ, 575, 435 (RSH02)

Shull, G. M., & van Steenberg, M. 1985, ApJ, 294, 599

Slettebak, A. 1982, ApJS, 50, 55

Smith, M. A., & Robinson, R. D. 1999, ApJ, 517, 866

———. 2003, in ASP Conf. Ser. 292, Interplay between Periodic, Cyclic, and Stochastic Variability, ed. C. Sterken (San Francisco: ASP), 263

Smith, M. A., Robinson, R. D., & Corbet, R. H. 1998, ApJ, 503, 877 (SRC98)

Smith, M. A., Robinson, R. D., & Hatzes, A. P. 1998, ApJ, 507, 945 (SRH02)

Szkody, P., et al. 2002, ApJ, 574, 942

van Steenberg, M., & Shull, G. M. 1988, ApJS, 67, 225

Warner, B. 1995, Cataclysmic Variables (Cambridge: Cambridge Univ. Press)

Waters, L. B., Cote, J., & Lamers, H. J. 1987, A&A, 185, 206

Waters, L. B., et al. 2000, in ASP Conf. Ser. 214, The Be Phenomenon in Early-Type Stars, ed. M. Smith, H. Henrichs, & J. Fabregat (San Francisco: ASP), 145